Journal of Energy Storage 21 (2019) 172–185

Contents lists available at ScienceDirect

Journal of Energy Storage

journal homepage: www.elsevier.com/locate/est

Battery energy storage system modeling: A combined comprehensive approach

Matthieu Dubarry[a,*], George Baure[a], Carlos Pastor-Fernández[b], Tung Fai Yu[c], W. Dhammika Widanage[b], James Marco[b]

[a] Hawai'i Natural Energy Institute, SOEST, University of Hawai'i at Mānoa, 1680 East-West Road, POST 109, Honolulu, HI, 96822, USA
[b] WMG, University of Warwick, Coventry, CV4 7AL, UK
[c] Jaguar Land Rover, Banbury Road, Warwick, CV35 0XJ, UK

ARTICLE INFO

Keywords:
Li-ion batteries
Cell-to-cell variations
Inhomogeneities
Pack modeling
Series
Parallel
BESS

ABSTRACT

Battery pack modeling is essential to improve the understanding of large battery energy storage systems, whether for transportation or grid storage. It is an extremely complex task as packs could be composed of thousands of cells that are not identical and will not degrade homogeneously. This paper presents a new approach toward battery pack modeling by combining several previously published models into a comprehensive framework. This work describes how the sub-models are connected, their basic principles, what adjustments were necessary, and what new parameters needed to be introduced. Overall, this paper introduces an open modular framework for future work on, among others, the impact of cell-to-cell variations, inhomogeneous degradation, SOC and SOH tracking, balancing and performance forecast.

1. Introduction

In recent years, there has been a great momentum of aggressive goals towards cleaner energy portfolios from stakeholders, local or federal. Per example, the state of Hawai´i have goals of 100% clean energy and transportation by 2045 [1,2]. With the projected high penetration of electric vehicles and electrochemical energy storage, there is a need to understand and predict better the performance and durability of large battery packs. Recent studies reiterated that batteries are susceptible to usage and that small differences in duty cycle could have a significant impact on the durability [3]. This precludes the use of black-box battery degradation models and highlights the need for a new battery pack model that can take all these aspects into consideration. This will prove especially valuable to assess the real impact/cost relationship of battery energy storage systems (BESS), new [4,5] or recycled [6], directly on the grid as well as in electric vehicles for driving or as grid support [7].

Battery pack modeling is intricate because of the number of parameters to consider. On top of an excellent single cell (SC) model, a battery pack model also needs to consider SCs small manufacturing and aging differences [8–17]. These slight variations could drastically influence the overall assembly performance and durability [18–21] and, as a result, all SCs should be considered independently while modeling the full system. Even with a perfect replication of the SCs, there are other parameters to consider with, among others, the cells imbalance, the topology (series and/or parallel), the temperature distribution, and the overall control scheme.

Looking at the literature, much work has been done for SC and pack modeling from a system perspective [22–25]. Most of the accurate SC models are using the Newman electrochemical model [26–30] or stochastic approaches [23,31]. Although accurate, and despite recent work on reduced ordered models [32], they are not convenient to scale up to the pack level because of calculation cost for modeling every SC individually. To deal with the added complexity of handing SC individually, most battery pack models are using multiple equivalent circuit models (ECM) connected in series or parallel [13,18,33–44].

From literature and previous experience, building blocks for an efficient BESS model that could scale up while considering SC variations, both intrinsic and aging-induced, without adding significant calculation time are available. However, they need to be combined to offer a unified model that could replicate the usage of batteries under any topologies and control strategies.

In this work, a new modular methodology for battery pack modeling is introduced. This energy storage system (ESS) model was dubbed *hanalike* after the Hawaiian word for "all together" because it is unifying various models proposed and validated in recent years. It

* Corresponding author.
E-mail addresses: matthieu.dubarry@gmail.com (M. Dubarry), C.Pastor-Fernandez@warwick.ac.uk (C. Pastor-Fernández), tyu5@jaguarlandrover.com (T.F. Yu).

https://doi.org/10.1016/j.est.2018.11.012
Received 21 August 2018; Received in revised form 8 November 2018; Accepted 8 November 2018

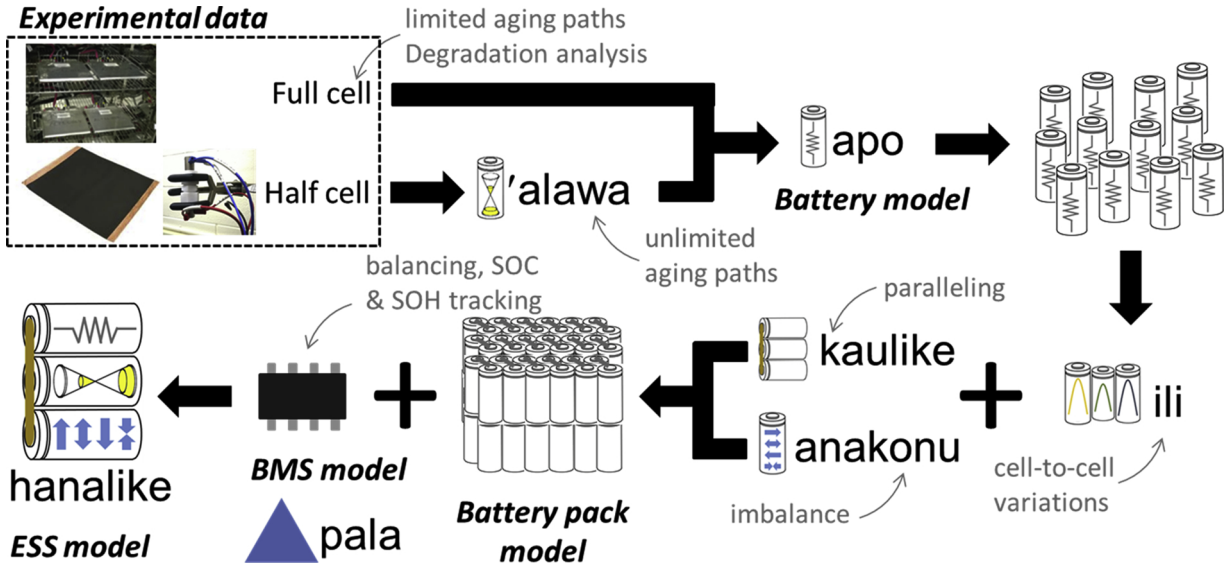

Fig. 1. Schematic view of the *hanalike* ESS model based on previously published sub-models, *'alawa* for degradation simulation [47], *apo* for ECM modeling of the single cells [45], *ili* for cell-to-cell variations simulation [34,46], *kaulike* for the paralleling calculations [40], *anakonu* for imbalance quantification [48], and *palapala'aina* (*pala* for short) for SOC and SOH online estimation [49].

Table 1
Summary of the sub-models included in the *hanalike* model.

Model's name (Hawaiian)	Level	Reference	Year	Functionality
Apo (English: circuit)	SC	[45]	2007	Calculates SC electrochemical behaviour
'Alawa (English: diagnosis)	SC	[47]	2012	Emulates SC voltage from half-cell data
Ili (English: distribution)	SC	[34,46]	2009	Accommodates cell-to-cell variations in *apo*
Anakonu (English: equilibrium)	Module	[40]	2015	Handles imbalance in series configuration.
Kaulike (English: parallel)	Module	[48]	2016	Handles imbalance in parallel configuration.
Palapala'aina (English: map)	SC	[49]	2017	Estimates state function (SOC and SOH) online.

comprises an ECM that can handle cell-to-cell variations [34,45,46], a model that can link voltage response and degradation [47], a model that can handle paralleling [40], a model that can quantify imbalance [48], and a model for online SOC and SOH estimation [49]. Fig. 1 presents a schematic view of the model and the interactions between the previously published sub-models, which are summarized in Table 1. In the *hanalike* ESS model, the SC models are based on the *apo* ECM model [45] and the data needed to parameterize could be gathered either from experimental testing or generated from *'alawa* simulations [47]. The response of the battery pack is calculated with cell-to-cell variations, topology, and imbalance took into consideration. The *ili* model handles one ECM per SC and is adjusting each parameter to handle cell-to-cell variations [34,46]. The *kaulike* model [40] handles paralleling, if necessary, and the *anakonu* model adjusts the SC state of charge (SOC) scales to account for imbalance [48]. The different battery pack state functions, such as the SOC and the state of health (SOH) [49], as well as the need for potential balancing, are determined by a modeled battery management system (BMS).

The present work introduces the core principles of this model built upon several published and well-validated sub-models [34,40,45–49]. The objective of this study is to discuss in detail how the different sub-models interconnect and what new parameters arise from these interactions. This new ESS model will be used as a framework to, among others, quickly evaluate the impact of SC inhomogeneities on pack performance and durability, the effect of temperature gradients on imbalance evolution, the influence of different balancing techniques, and the accuracy and feasibility of SOC or SOH estimation techniques. Several studies are under way to validate the approach further and demonstrate its capability. A subsequent publication will highlight the use of this model as a diagnostic tool for inhomogeneities at the time of module or pack assembly.

2. Model description

Fig. 2 presents the model algorithm. The simulation starts with the first step of the requested duty cycle at a time $t = 0$. The model first calculates the full electrochemical response of all SCs independently based on their characteristics and their SOH (SC engine). This will be repeated at every SOH. Each of the SC ECMs can be parameterized either from experimental data or half-cell data as well as offline or online (real-time). Once the SC electrochemical behaviors are established, the model merges them to predict the pack voltage (V), current (I), and temperature (T) after the application of the duty cycle for an iteration of time ε (Pack engine). If some cells or modules are in parallel, the calculation is done via the paralleling sub-model; otherwise, the SC models are simply added after SOC correction from imbalance. The cells imbalance parameters (scaling and translation factors [48]) are calculated from the SOC and capacity ration at the SC and module levels (Pack engine). The final phase of each iteration of the model corresponds to the controls (BMS engine). If the V, I, and T at time $t+\varepsilon$

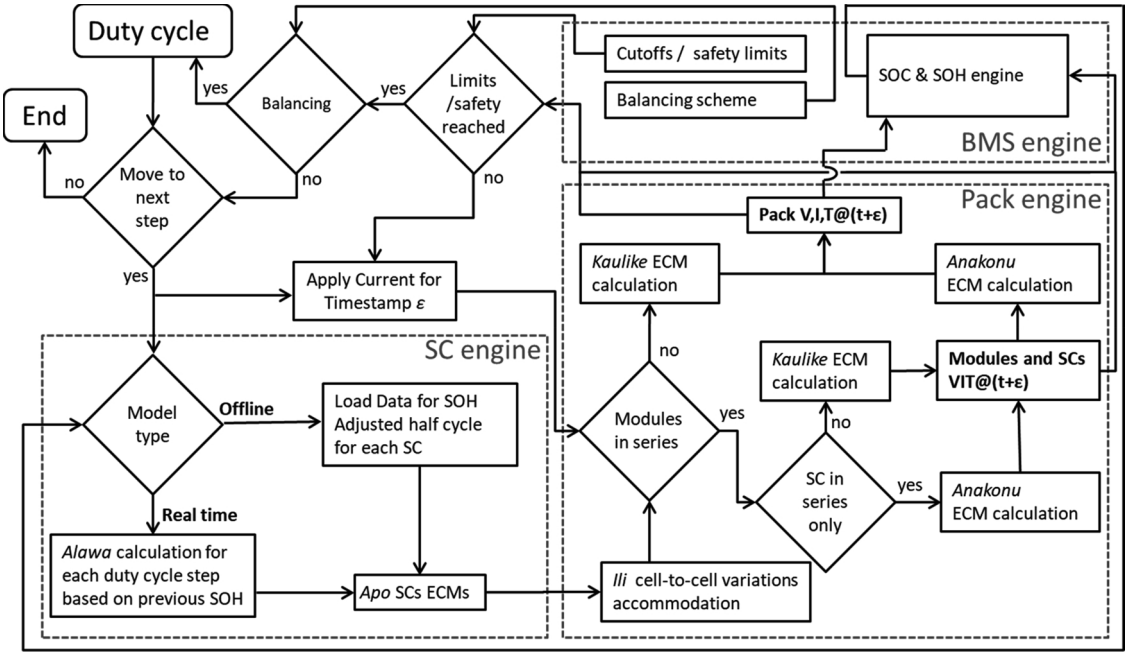

Fig. 2. Hanalike ESS model algorithm highlighting the different calculation engines for the single cells, the modules, the full pack, and the battery management system.

reached a cutoff or safety limit, the step is terminated. If the conditions for a balancing step or an update in protocols are met, the duty cycle is modified to incorporate the balancing currents. This process is repeated until the duty cycle is simulated in its entirety. The choice of duration for ε is a balance between accuracy and calculation time. The next sections will provide more details on the three main calculation engines: single cell, pack, and BMS as well as a discussion of different key parameters.

2.1. Single cell engine

The purpose of the SC engine is to calculate the global electrochemical behavior and performance of each SC independently at any given step of the duty cycle. It uses the *apo* modified ECM, the '*alawa* model, and feedback from the pack and BMS engines for temperature and SOH.

2.1.1. Apo ECM sub-model

The *apo* model is a generic ECM model with a variable R_2 resistance in parallel with a capacitance (Cap). It was shown to offer high fidelity over the entire SOC and current range [45]. This ECM uses data from a few rates, from low to high, to calculate any intermediate rates via bilinear interpolation [45].

Fig. 3 presents a schematic of how the ECM is parameterized. Data at several rates in charge and discharge is used to decipher three parameters, the open circuit voltage (OCV), and two resistances, R_1 and R_2. A pseudo−OCV curve, obtained by averaging the low rate charge and discharge [50,51], can be used instead of the real OCV curve. The resistance R_1 can be obtained from the IR drop measurable when current is first applied [46]. Finally, once R_1 and the OCV are deciphered, R_2 can be calculated by subtracting R_1 from the overall polarization at each SOC for every tested rate [45]. The value of Cap, in F, can be obtained from impedance spectroscopy for short time periods or from DC pulses techniques for longer ones. With the OCV, R_1, R_2, and Cap known, the voltage as a function of time can be calculated using Eq. (1) [52,53] with $Q_{cap}(0)$ being the initial charge of the capacitor.

$$V(t+\varepsilon) = \frac{Q_{Cap(0)}}{Cap} e^{-\frac{t}{R_2 Cap}} + OCV - I(t)R_1 - \left(1 - e^{-\frac{t}{R_2 Cap}}\right) I(t)R_2 \quad (1)$$

All parameters in Eq. (1) vary with T and SOH. OCV, R_2, and Cap also vary as a function of SOC. R_2 is the only parameter that varies as a function of I as well. The entire parameterization process then needs to be repeated at different SOHs and temperatures to build a set of look-up tables with the variations of R_1, R_2, OCV, and Cap. This will allow the ECM to calculate the SC behavior under any conditions (SOC, SOH, I, T) within the SOC and current range that was tested. More details on this approach and its validation can be found in [45,46].

2.1.2. 'Alawa sub-model

As mentioned in the previous section, some extensive voltage vs.

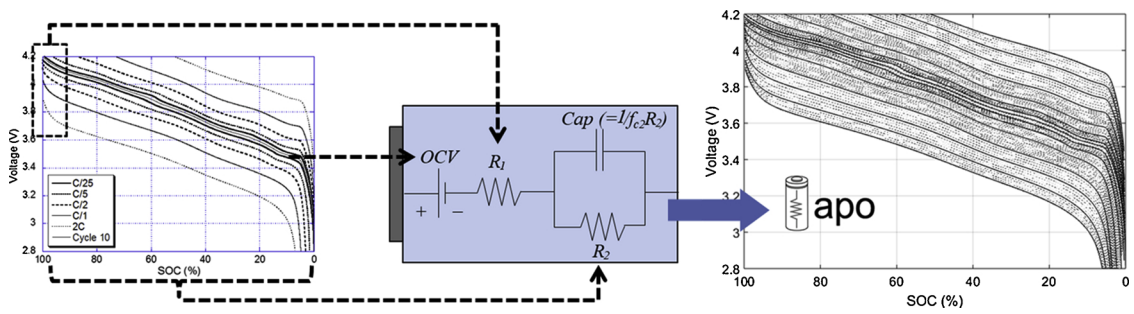

Fig. 3. Schematic representation of the *apo* ECM model [45].

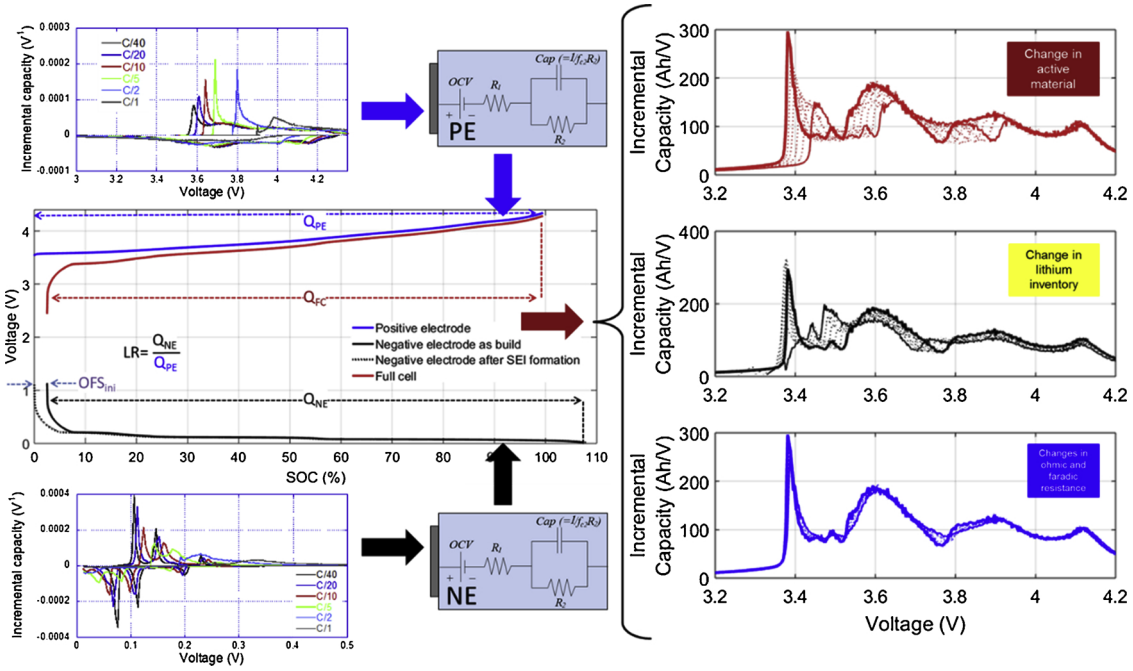

Fig. 4. Schematic representation of the '*alawa* model [47].

SOC data is needed to parameterize the ECM, especially for multiple SOHs and temperatures. This data can be obtained from laboratory testing by cycle aging cells while performing periodic reference performance tests. The drawback of this approach is that the obtained model relies on interpolations and more importantly is bounded by the tested conditions (duty cycle, rates tested and temperatures). Indeed, the degradation, and thus the SOH, only reflects the experimental aging scenario and nothing else. In this case, the only degree of freedom for the model in terms of degradation is its pace. Such predefined degradation will be qualified as "offline" in the rest of this work.

To gain more flexibility in the possible aging scenarios, the data collected above can be used differently with the '*alawa* approach [47] in which data from pristine positive and negative electrodes (PE and NE respectively) are compiled to emulate the behavior of the full cell (FC). This emulated cell can then be used to simulate different SOHs or temperatures. The '*alawa* approach was described in detail before [47,54] and validated by independent studies [55–57]. This approach is summarized in Fig. 4. First, the PE and the NE need to be harvested from a fresh cell and tested against metallic lithium at different rates. This data is used in conjunction with the ECM to create a model per electrode (each containing multiple ECMs for composite electrodes). The electrode OCVs are then matched to replicate the electrochemical behavior of the full cell by fitting two parameters, the initial loading ratio (LR_{ini}), the capacity ratio between the two electrodes, and the initial offset (OFS_{ini}), the electrode slippage induced by the initial solid electrolyte interphase layer formation. An example of the relationship of the full cell OCV, the positive and negative electrode OCVs as well as LR and OFS is provided in Eq. (2) in the case where the positive is limiting in charge, and the negative is limiting in discharge, the most likely scenario in today's graphite-based commercial Li-ion cells.

$$OCV_{FC}(SOC_{FC}) = OCV_{PE}(SOC_{FC}.(1-OFS)+OFS) - OCV_{NE}\left(1 - SOC_{FC}\frac{1-OFS}{LR}\right) \quad (2)$$

Varying LR and OFS allow the simulation of different SOHs from pristine half-cell data. Battery degradation can always be decomposed into contributions from three categories: loss of lithium inventory (LLI), loss of active material (LAM) and change of kinetics [54,58–60]. Any change in the cell SOH will change the balance of the electrodes and translate in a change in LR and OFS [47] from which LLI and LAM on each electrode can be quantified [47] by Eqs. (3) and (4). A methodology to handle changes of resistance and electrode kinetics was also proposed using two parameters, the ohmic resistance increase (ORI) and the rate degradation factor (RDF), Eqs. (5)–(7). This allows simulating kinetic and resistance changes as well as different temperatures from room temperature data. More details on the different equations can be found in [47].

$$LR = \frac{100\% - \%LAM_{deNE} - \%LAM_{liNE}}{100\% - \%LAM_{dePE} - \%LAM_{liPE}} LR_{ini} \quad (3)$$

With de- and li- standing for delithiated and lithiated, respectively.

$$OFS = OFS_{ini} + LR\,\%LAM_{liNE} - \frac{LR}{LR_{ini}}\%LAM_{dePE} + \%LLI_{ch} - \%LLI_{dis} \quad (4)$$

$$C_{PE} = \frac{100\%\,RDF_{PE}\,C_{Req.}}{100\% - \%LAM_{dePE} - \%LAM_{liPE}} \quad (5)$$

$$C_{NE} = \frac{100\%\,RDF_{NE}\,C_{Req.}}{LR_{ini}(100\% - \%LAM_{deNE} - \%LAM_{liNE})} \quad (6)$$

$$V_{cell}@C_{Req.} = V_{PE}@C_{PE} - (R1_{PE} + R2_{PE})C_{PE}\left(\frac{\%ORI_{PE}}{100\%} + RDF_{PE} - 1\right) - V_{NE}@C_{NE} + (R1_{NE} + R2_{NE})C_{NE}\left(\frac{\%ORI_{NE}}{100\%} + RDF_{NE} - 1\right) \quad (7)$$

Where $C_{req.}$, C_{PE}, and C_{NE} are the requested rate and the rate on the positive and negative electrode, respectively.

Using the '*alawa* approach, it is possible to predict the cell voltage response under any possible degradation, and thus associated OCV, R_1, and R_2, from one set of pristine half-cell data. Coupled with the ECM, '*alawa*-based SC models under specific degradation mechanisms can then be calculated offline to offer different predefined degradation paths such as different calendar aging conditions. It must be noted that the current and temperature ranges that can be simulated depends on the current ranges tested on the half-cells.

The '*alawa* approach can also be used online in real time, without

Table 2
Input and output parameters for the single cell engine.

Input Parameters	Description
Cap	Capacitance. Obtained from EIS spectroscopy
T^k	Temperature of all k single cells
Option 1	
V_{FC} vs. SOC	Voltage of the cell to simulate under different rates and temperatures at different SOHs
$SOH_{SC}{}^k$	SOH for all k single cells
Option 2	
V_{PE} vs. SOC	Voltage of the pristine PE under different rates
V_{NE} vs. SOC	Voltage of the pristine NE under different rates
LR	Loading ratio between the PE and the NE
OFS	SOC offset between the PE and the NE
ORI_{NE}/ORI_{PE}	Ohmic resistance increase for the NE / PE
RDF_{PE} /RDF_{PE}	Rate degradation factor for the NE / PE
Ouput Parameters	Description
$V_{SC}{}^k$ vs. SOC	Voltage vs. SOC vs. C for all k single cells at their respective SOH and temperature.

any precalculation, if the relationships between degradation and different parameters are known (e.g., %LLI per cycle as a function of current and temperature). The BMS engine can, for each iteration, calculate the change in parameters associated with the operating conditions for each SC and feed that information to the SC engine to update each model individually. This allows unprecedented flexibility in studying the impact of inhomogeneities in aging.

2.1.3. SC engine parameterization

The SC engine is composed of two sub-models, the *apo* ECM and *'alawa*. If used from experimental full cell data at different rates and temperatures, only the ECM is needed to calculate the SC voltage responses at their current SOH and temperature. If used from electrode half-cell data with a predefined degradation, the ECM is used to simulate each individual electrode and *'alawa* is used to match them to emulate a full cell at a given SOH and temperature. If used in real time, the electrode ECM models are fed with BMS calculated values of ORI, RDF, LR and OFS for each iteration of SOH. Table 2 summarizes the different parameters needed to execute the SC engine: Option 1 corresponds to a model based on experimental data or precalculated *'alawa* data and Option 2 corresponds to a model based on real time *'alawa* data. If Option 2 is chosen and if one of the electrodes is a composite, each phase of the composite requires its own set of parameters.

2.2. Pack engine

The purpose of the pack engine is to consider the cell-to-cell variations, the imbalance as well as the pack and module topologies to calculate the voltage, current, and temperature changes associated with the application of a duty cycle step for a time ε. It uses input from the SC engine as well as the *ili*, *anakonu*, and *kaulike* sub-models.

2.2.1. Ili sub-model

The *ili* sub-model enables the SC models to all be slightly different depending on cell-to-cell variations. To do so, the model adjusts up to eight parameters for every single cell. This includes R_1, and the initial SOH (SOH_{ini}) but also the capacity ration Qr and the rate capability RC. Qr, in mAh/%SOC, quantifies the relationship between capacity and SOC and represents 1% of the SC maximum capacity. RC is a proxy to the SC kinetics. In this work, it corresponds to the ratio of the nominal capacity to the maximum capacity. If the SC models are real time *'alawa*-based, thermodynamic variations in LR and OFS also need to be considered [49], and the variations in ohmic resistance and rate capability need to be translated to variations in ORI and RDF for both the PE and the NE (Eqs. (5)–(7)).

All parameters listed above, to the exception of SOH_{ini}, correspond to manufacturing cell-to-cell variations [12,17,61]. Looking at the ECM, Fig. 3, the accommodation of R_1 for every single cell is straightforward because it is a direct model parameter (Eq. (1)). However, the accommodation of the others is more complex. Changes in LR and OFS requires adjustments of the OCV function (Eq. (2)). Changes in Qr and RC requires adjustments in other parts of the model. For offline models, the rate table in the ECM needs to be adjusted to reflect the fact that the maximum capacity and the capacity at the nominal rate changed. Fig. 5 presents an example of RC adjustments for a graphite // $LiNi_xAl_yCo_{1-x-y}O_2$ battery showcasing how (a) the model scales the rate table and (b) how the voltage response at the nominal rate is modified when the RC is adjusted. For real time models, RDF in Eqs. (5)–(7) needs to be adjusted. For example, if a SC kinetic is slower than average, a C/2 might need to be simulated as a C/1.5 with a resistance adjustment so that the polarization still corresponds to a C/2 rate and not a C/1.5 [47].

The last parameter to consider is SOH_{ini}. For offline SC models, a SC behavior is precalculated for every cycle until the capacity reached 0. Therefore, data at different SOH is available with a resolution that equals to 100 divided by the number of cycles the cell was tested/simulated. In other words, if the SC model is set so that 90%SOH is reached after 100 cycles, each cycle, and thus the SOH resolution, corresponds to 0.1% SOH. To accommodate changes in SOH_{ini}, the

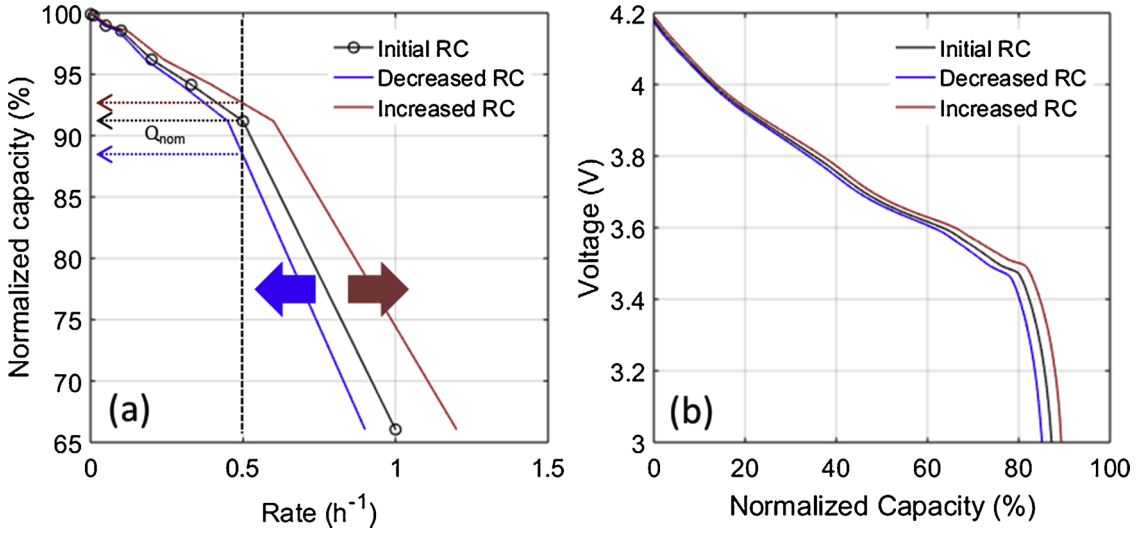

Fig. 5. (a) Example of RC accommodation and (b) resulting voltage response at C/2.

model will change the starting cycle for each SC model. For a 0.1% SOH resolution and a starting SOH of 99% instead of 100%, the model for cycle ten will be used in lieu of the model for cycle 1. For step-by-step real-time degradation models, the changes in SOH_{ini} are handled with changes in '*alawa* parameters (cf. Section 2.1.2).

2.2.2. Anakonu sub-model – Cells or modules in series

The *anakonu* model [48] characterizes imbalance by deciphering two parameters for each SC, the scaling factor, and the translation factor. Based on these factors, the signature of the battery pack can be calculated from the SCs using a simple set of equations, Eqs. (8)–(12) [48]. The open pack voltage (OPV) can be expressed as a function of the OCV of all the SC comprising the pack according to Eq. (8). To account for imbalance, the OCVs of the different SCs need to be scaled or translated against each other. This is done with the scaling and translation factors defined in Eqs. (9) and (10). The scaling factor can be directly calculated from a normalization of the Qr of every SC to the Qr of the 1st cell in the pack [48]. The translation factor depends on the SC SOCs at any given time. At $t = 0$, the only input parameter needed is thus the SC initial SOCs (SOC_{ini}) since the Qrs are available from the SC models.

$$OPV\,({}_{SC1}SOC) = {}_{SC1}OCV\,({}_{SC1}SOC) + \sum_{i=2}^{n} {}_{SCi}OCV\,({}_{SCi}\mathrm{sf}({}_{SC1}SOC + {}_{SCi}\mathrm{tf})) \tag{8}$$

With

$${}_{SCi}tf = {}_{SC1}SOC - {}_{SCi}SOC \tag{9}$$

And

$${}_{SCi}sf = \frac{{}_{SCi}Qr}{{}_{SC1}Qr} \tag{10}$$

Eq. (8) is relative to the SOC of the first SC. A rescaling, Eq. (11), is necessary to compute the SOC of the pack from the SOC of the SC and the pack cutoff voltages. Additionally, once the SOC of the pack is calculated, it can be used to calculate the pack capacity ration according to Eq. (12). More details on the equations and their validation can be found in [48].

$${}_{pack}SOC = \frac{{}_{SC1}SOC - {}_{SC1}SOC\,(Cutoff_{discharge})}{{}_{SC1}SOC\,(Cutoff_{charge}) - {}_{SC1}SOC\,(Cutoff_{discharge})}\,100\% \tag{11}$$

$${}_{pack}Qr = \frac{{}_{SCi}SOC\ {}_{SCi}Qr}{{}_{pack}SOC} \tag{12}$$

The principles of the model are graphically represented in Fig. 6 for a 3S1P configuration. Assuming that two rest cell voltages are available and that the capacity exchanged between them is known, the signature of the pack can be calculated by vertically aligning the blue boxes that represent each SC ΔSOC. On the left of Fig. 6 it can be seen that the three cells have different Qr as, for the same exchanged capacity, the ΔSOC (the size of the blue box) is different. By applying a scaling and a translation, the blue area under all three curves can be aligned (Fig. 6 right). Once aligned, the voltage curves can be summed vertically to calculate the battery pack signature despite differences in Qr, OCV curves, SOH, and initial SOC. When published and validated [48], the model was only used with OCV curves. Coupled with the ECM and the cell-to-cell variation accomodation, the match of the OCV curves can now be used to calculate the electrochemical response at other rates.

2.2.3. Kaulike sub-model – Cells or modules in parallel

The *kaulike* paralleling model [40] uses the ECM and Eq. (1) as a base. The concept is to determine the intersection of voltage vs. rate curves for each SC in an assembly based on their current SOC and derive the transient balancing current and the voltage. Fig. 7 illustrates the paralleling approach with an example of two cells in parallel, one with a low SOC and one with a high SOC. Based on the ECM, it is possible to calculate the voltage as a function of the rate for both cells at their given SOCs. Plotting these voltage vs. rate curves on the same scale relates the rate on the SC to the rate on the assembly. Knowing the rate on the assembly, the balancing current and voltage for a time step ε can then be deciphered. The same calculation is repeated for each model iteration with updated SOCs. For strings of cells, the voltage vs. rate curves are calculated for the entire strings. More details and validation can be found in [40].

2.2.4. Pack engine parameterization

The pack engine is composed of three sub-models, the *ili* cell-to-cell variation accommodator, the *kaulike* paralleling model and the *anakonu* imbalance model. The *ili* model is taking the SC models from the SC engine and is tuning them to account for cell-to-cell variations. Based on the pack and module topologies, the most adapted sub-models, between *kaulike* and *anakonu*, will be used to calculate the voltage, the current and the temperature at time $t+\varepsilon$ under the conditions defined by the present step of the duty cycle (constant current, constant power, …). Table 3 summarizes the different input parameters needed to make that calculation possible.

2.3. BMS engine

In the previous sections, a set of sub-models was used to calculate the electrochemical behavior of the battery pack to determine V, I, and T (to be implemented) as a function of the requested duty cycle for an iteration of time. The BMS engine is independent and has three completely separate tasks:

- Determine if any cutoffs were reached during the time step and thus whether to continue the present step, move to the next step, or modify the duty cycle (to introduce some balancing or to protect the cells). The cutoffs and safety limits could be pack, module, or SC-related and time, voltage, current, temperature, or capacity based.
- Prepare for the next iteration by computing the changes in SOH associated with the current iteration.
- Perform some classic BMS functions such as using some algorithms, e.g. [49], to track SOC and SOH from the electrochemical response of the pack. This task is completely independent from the others and is not necessary for running the model.

Depending on the model type (offline or real-time), SOH changes are handled in different ways. For offline degradation, the SOH changes could be cycle based or total exchanged SOC based (i.e., relative to the capacity throughput). Aging variations between cells [11,16,62,63] are introduced via a ponderation factor (ΔSOH) on the cycle number to use for the simulation. For a cell that degrades 10% faster than the reference cell, cycle 110 will be used to simulate cycle 100. For real-time step-by-step degradation, the BMS module needs to store the different equations that relate aging factors (temperature, current, voltage, ΔSOC, time,… [64]) to degradation and calculate the associated changes in '*alawa* parameters (LR, OFS, ORI, RDF) for each step. These equations can be determined experimentally or with the use of high fidelity electrochemical models. Taking an example, it was found that for calendar aging of a commercial graphite / $LiNi_xAl_yCo_{1-x-y}O_2$, LLI and LAM_{PE} could be estimated from the temperature, the SOC and the time using a double quadratic model (Eq. (2) in [65]), [65,66].

There is another essential set of parameters to take into account in order to determine the SOH of the pack from the SOH of the SCs: the ratio of degradation in charge vs. discharge. Although it does not influence the SC signature, whether the degradation appeared during discharge or charge will influence the signature of the pack because if will induce imbalance in the absence of balancing. This will be discussed further in Section 3.3.

Table 4 summarizes the main parameters needed to execute the

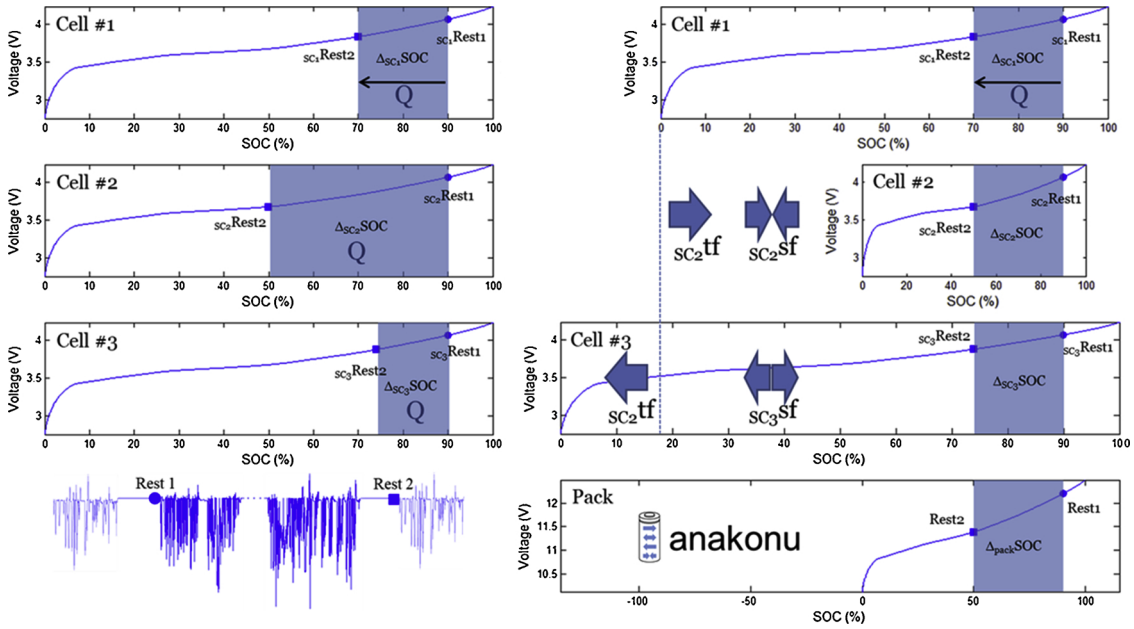

Fig. 6. Schematic representation of the *anakonu* imbalance model [48].

BMS engine in the case of a predefined degradation. For a step-by-step degradation, a set of equations linking usage and '*alawa* parameters is also needed.

3. Discussion

All the sub-models used in this work were previously published and validated [34,40,45–48]. This new "all together" model was successfully tested against all the experimental validation used in the above-mentioned publications, and this will not be further discussed in this work. It appeared more important to discuss further the novelty of several aspects of this model: The emulation of OCV curves for offline degradation, the ability for *'alawa* to emulate different temperatures, the importance of defining if the degradation happened in charge or discharge, the opportunity for electrochemical voltage spectroscopies (EVS), as well as some of the model limitations and possible applications.

3.1. Emulation of OCV curves in-between reference perfromance tests

For the ECM offline models that are based on experimental data, only a few cycles are available since reference tests are usually performed, at best, every 100 cycles. In this ESS model, the SOH is calculated cycle by cycle and therefore there is a need for interpolation in-between reference tests for all the parameters in Eq. (1) (R_1, R_2, C, OCV, Qr and RC). For SOC-independent parameters, a simple linear interpolation is used. For SOC-dependent parameters, a choice between interpolation on the voltage and SOC axis is needed to be able to accommodate for the complex changes with SOC depending on the cell chemistry.

For instance, voltage plateaus in OCV curves can change in multiple ways (voltage, slope, length…) upon aging depending on the degradation mechanism and/or the chemistry. Fig. 8 displays the evolution of the OCV curves for simulated Graphite//$LiMn_2O_4$ (LMO) and Graphite//$LiFePO_4$ (LFP) cells, the details from which can be found in [48,67]. Fig. 8(a) and Fig. 8(b) shows the changes in the OCV signature for the LMO and LFP cells, respectively, up to 20% LLI with 5% increments as calculated from the *'alawa* toolbox. It can be seen that the OCV curves are not varying the same way and that, for the LMO cell (arrow on Fig. 8(a)) the voltage of the plateaus is changing; whereas, for the LFP cell (arrow on Fig. 8(b)), the SOC range of the plateaus is changing. Linear interpolations will only be able to capture one or the other depending on which axis (voltage or SOC) is used. To further demonstrate the impact of the interpolation technique, Fig. 8(c) and (d) compares the SOC error associated with interpolated OCV curves after 5, and 15% LLI for the LMO and LFP cells, respectively. The average SOC estimation error is always below 0.5% for all methods, but, as expected, SOC interpolation is better than the voltage interpolation for the LMO cell (average of 0.17% vs. 0.22% with maximums at 0.85% vs. 1.2%), and the opposite is true for the LFP cell (average error of 0.1%

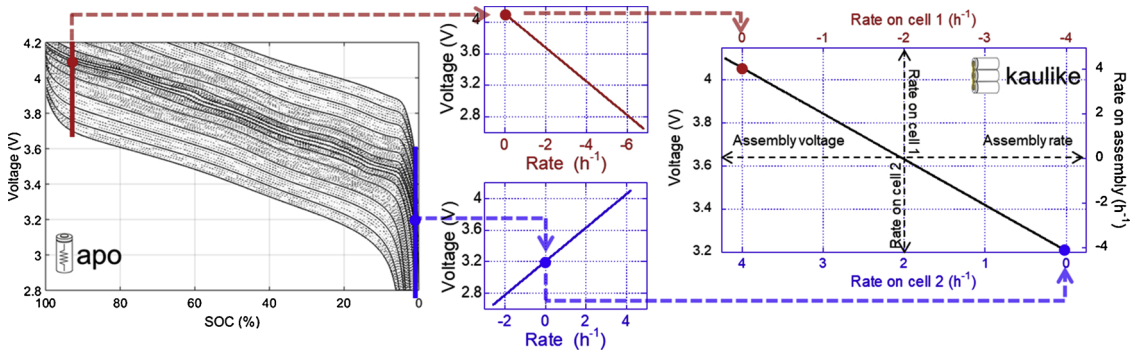

Fig. 7. Schematic representation of the *kaulike* paralleling model [40].

Table 3
Input and output parameters for the pack engine.

Input Parameters	Description
I_{req}	Requested rate
ε	Time iteration duration
Qr^k	Capacity ration for *k* SCs
R_1^k	R_1 resistance for *k* SCs
RC^k	Rate capability for k SCs (Q_{nom}/Q_{max})
LR^k	LR for *k* SCs
OFS^k	OFS for *k* SCs
SOH_{ini}^k	Initial SOH for *k* SCs
SOC_{ini}^k	Initial SOC for *k* SCs
$Topo_{Mod}$	Module topology
$Topo_{Pack}$	Pack topology
$Cutoff_{Pack}$	Pack voltage cutoffs
Ouput Parameters	Description
$V_{SC}^k(t+\varepsilon)$	Voltage for all k single cells at time t+ε.
$OCV_{SC}^k(t+\varepsilon)$	OCV for all k single cells at time t+ε.
$I_{SC}^k(t+\varepsilon)$	Current for all k single cells at time t+ε.
$SOC_{SC}^k(t+\varepsilon)$	SOC for all k single cells at time t+ε.
$Qr_{SC}^k(t+\varepsilon)$	Qr for all k single cells at time t+ε.
$T_{SC}^k(t+\varepsilon)$	Temperature for all k single cells at time t+ε.
$V_{Mod}^j(t+\varepsilon)$	Voltage for all j modules cells at time t+ε.
OCV_{Mod}^j (t+ε)	OCV for all j modules at time t+ε.
I_{Mod}^j (t+ε)	Current for all j modules at time t+ε.
SOC_{Mod}^j (t+ε)	SOC for all j modules at time t+ε.
Qr_{Mod}^j (t+ε)	Qr for all j modules at time t+ε.
T_{Mod}^j (t+ε)	Temperature for all j modules at time t+ε.
$V_P(t+\varepsilon)$	Voltage for the pack at time t+ε.
OPV (t+ε)	OPV for the pack at time t+ε.
I_p (t+ε)	Current for the pack at time t+ε.
SOC_p (t+ε)	SOC for the pack at time t+ε.
Qr_p (t+ε)	Qr for the pack at time t+ε.
T_p (t+ε)	Temperature for the pack at time t+ε.

Table 4
Input and output parameters for the BMS engine for a predefined degradation.

Input Parameters	Description
$Cutoffs_{SC}$	SC voltage / current / temperature cutoffs
$Cutoffs_{Mod}$	Module voltage / current / temperature cutoffs
$Cutoffs_{Pack}$	Pack voltage / current / temperature cutoffs
$Cutoff_{cond}$	Cutoff condition (SC, module or pack)
$Safety_{SC}$	SC voltage / current / temperature safety cutoffs
$Safety_{Mod}$	Module voltage / current / temperature safety cutoffs
$Safety_{Pack}$	Pack voltage / current / temperature safety cutoffs
ΔSOH^k	Aging variability for *k* SCs
$\%deg_{cha}^k$	Percentage of degradation in charge for *k* SCs
$\%deg_{dis}^k$	Percentage of degradation in discharge for *k* SCs
Ouput Parameters	Description
Balancing I/O	Balancing signal
Cutoff I/O	Cutoff signal
SOH_{SC}^k	SOH for all k single cells (option 1)
LR t+ε)	Loading ratio at time t+ε (option 2)
OFS t+ε)	SOC offset at time t+ε (option 2)
$ORI_{NE/PE}(t+\varepsilon)$	ORI for the NE / PE at time t+ε (option 2)
$RDF_{PE\ /PE}(t+\varepsilon)$	RDF for the NE / PE at time t+ε (option 2)
SOC_p^{BMS}	Pack SOC as measured by BMS
SOH_p^{BMS}	Pack SOH as measured by BMS

vs. 0.33% with maximums at 0.5% vs. 1.8%). This was also verified by experimental data where OCV curves were available every five cycles [67] (not shown). The further apart the reference tests are, the more the difference will be pronounced.

3.2. Emulation of temperature from room temperature data

Based on Eqs. (5)–(7), the resistance and the kinetics of cells can be accommodated. Since it is known that temperature induces changes in resistance and kinetics, it might then be possible to emulate changes in temperature from data gathered at 25 °C. As a proof of concept, Fig. 9(a) presents the comparison of a commercial graphite/LMO cell (from [48]) cycled at 2C and 60 °C to ECM simulations of the same cell at 2C, C, and C/2 at room temperature. The 2C simulation at room temperature is dissimilar to the experimental one because of the temperature effect. Looking closer at the voltage response of the cell, the 2C at 60 °C curve resembles the C/2 at 25 °C curve from simulation except for the ohmic resistances that are different. By adjusting the resistance so that both discharges start at the same voltage, Fig. 9(b), it can be seen that the IC curves are indeed rather similar. Therefore, it might be possible to emulate a 2C discharge at 60 °C by simulating a C/2 discharge at room temperature with a higher than average resistance. Additional work is in progress to verify this hypothesis and to investigate different rates and temperatures to understand better how to parameterize changes in temperature in the ECM and *'alawa*.

3.3. Degradation in charge or discharge

One of the new parameters introduced in this work are factors indicating whether the degradation is occurring mostly in the charge or the discharge regime. The same parameters could also be described as low/high SOC degradation for complex duty cycles (e.g., pulses). A schematic representation of the impact of discharge, charge, and 50/50 discharge/charge degradation is presented in Fig. 10(a–c, respectively) where the initial OCV, as well as the OCV after 5%, 10%, 15%, and 20% capacity loss, are plotted against normalized initial capacity. If the degradation is occurring in discharge, Fig. 10(a), the beginning of discharge capacity is always the same, but the normalized capacity at the end of discharge is getting higher and higher. If the degradation is occurring in charge, the end of discharge capacity remains constant, and the capacity at the end of charge is getting lower and lower, Fig. 10(b). If the degradation is happening during charge and discharge, both the capacity at the end of discharge and the end of charge will change, Fig. 10(c).

In all three cases, the OCV curves versus SOC and the capacity loss on the SCs are the same after aging. Therefore, at the SC level, it does not matter where the degradation is occurring, and as a result, this parameter was, to the best of our knowledge, never described. At the pack level, the location of the degradation is going to play a prominent role in the evolution of the imbalance of the assembly. Indeed, if cells degrade at a different pace (i.e., with different ΔSOH), they will reach different SOCs at the end of charge and/or end of discharge. Fig. 10 takes the example of a 100S1P battery pack with ± 30% ΔSOH after 25% capacity loss with the distribution of the beginning and end of discharge SOC for (d,e) degradation in discharge, (f,g) degradation in charge and (h, i) a 50/50 degradation. In all three cases, the spread of SOCs after aging are different, and thus the evolution of imbalance was different. This complexity is often mitigated by balancing, but it is visible where no balancing is involved as exemplified by [21] for an LFP battery pack. Balancing at the end of discharge will favor case (b). Balancing at the end of charge will favor case (a).

How to assess these percentages from experimental data is yet to be established. A possibility could be to track capacity slippage upon cycling. Looking back into recently published 4S1P battery pack data [68], Fig. 11, and plotting the voltage vs. capacity response of the pack for the entire 50 cycles; it can be seen that the curves are slipping to the left. This is mostly induced by the slight difference in coulomb counting between the charge and the discharge and the lack of high precision coulometer [69,70]. For the room temperature pack, Fig. 11(a), the slippage at the end of charge came to -0.505 Ah after 50 cycles vs. -0.439 Ah at the end of discharge. If no capacity was lost, and slippage only induced by a calibration error, the slippage should have been the same at the end of charge and discharge. The fact that the end of discharge slipped 0.066 Ah less (2.5% of the cell capacity, close to the observed capacity loss of 3%) suggest that the degradation likely occurred mostly during discharge because less capacity was discharged than charged. Looking at the pack that was cycled at 0 °C, Fig. 11(b), the evolution of the slippage is much more complicated. Slippage was of

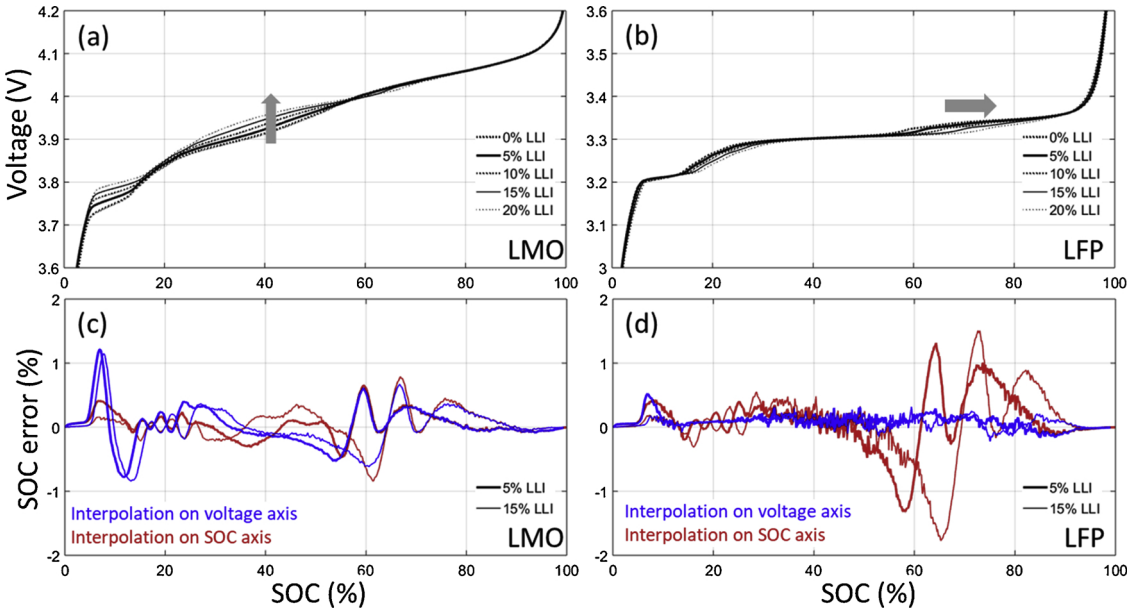

Fig. 8. OCV variations for up to 20% LLI for (a) a Graphite//LMO cell and (b) a Graphite LFP cell. OCV estimation errors at 5% and 15% LLI based on interpolation on a voltage axis or the SOC axis for (c) the Graphite//LMO cell and (d) the Graphite//LFP cell.

-0.779 Ah at the end of charge and + 0.732 Ah at the end of discharge after 50 cycles. Assuming a similar calibration error than of the other test, the degradation induced slippage was of -0.274 Ah at the end of charge and + 1.170 Ah at the end of discharge. This accounts for 62% of the cell capacity, close to the observed 66% capacity loss. This also implies that, for this pack, 80% of the capacity was lost in discharge and 20% in charge, thus in a different fashion than the room temperature pack. This method seems to give trends on where the degradation occurred. Some tests on high-resolution battery coulombmeters [69,70] could help validating the approach further.

3.4. Electrochemical voltage spectroscopies at the pack level

One of the benefits of this approach is to be able to apply EVS [71,72] at the battery pack level and be able to relate the observations at the SC level. To the best of our knowledge, few studies reported the EVS signature of battery packs upon aging [73]. This is probably due to the complexity of the electrochemical response. The relationship between the pack incremental capacity (IC_P, dQ_P/dV_P) and differential voltage (DV_P, dV_P/dQ_P) signatures and the SC ones is convoluted because, for each dV_P or dQ_P of the pack, each SC could have their dV_{SC} and dQ_{SC}. However, there are two exceptions where the relationship between the pack and the SC signatures is easy to decipher: when cells are either all in series or all in parallel. If the cells are all in series, the pack and the SC experience the same change of capacity dQ and therefore, since they have the same denominator, the DV curve of the pack corresponds to the sum of the DV curves of the SCs. If the cells are all in parallel, the pack and the SC experience the same change of voltage, dV, and therefore, since they have the same denominator, the IC curve of the pack corresponds to the sum of the IC curves of the SCs. Every other case is much more complex. Despite the complexity, the IC and DV relationship can be derived numerically and plotted, Fig. 12. Fig. 12(a) shows the IC signature in the discharge of a 49S1P battery pack, dQ_P/dV_P, composed of graphite/$LiMn_2O_4$ cells with up to 10% difference in their initial SOC. Fig. 12(b) displays the IC curves of the SC within the pack versus the pack voltage, dQ_{SC}/dV_P, and Fig. 12(c) the same IC signature versus their own voltage, dQ_{SC}/dV_{SC}. The impact of the SOC imbalance on the SC usage is

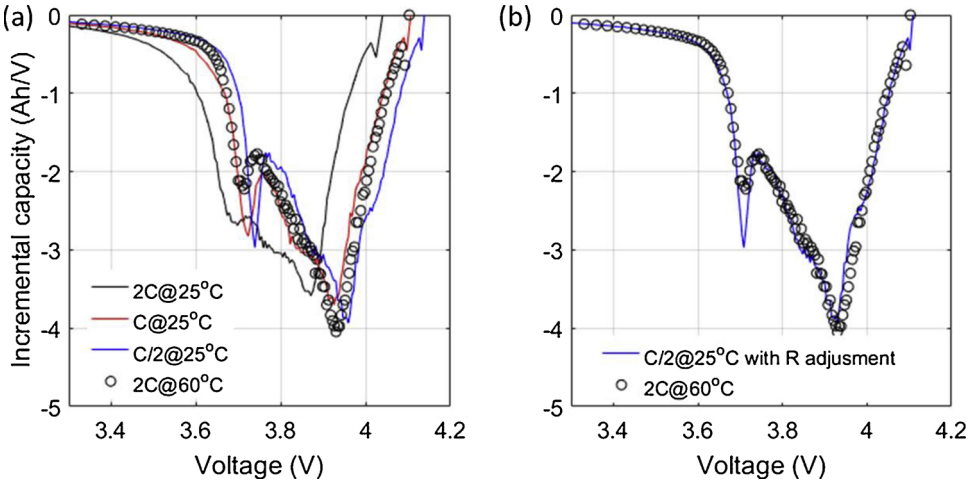

Fig. 9. (a) Incremental capacity signature of ECM modeled graphite//$LiMn_2O_4$ commercial battery at different rates compared to experimental data at 2C and 60 °C. (b) Comparison of the emulated C/2 discharge at 25 °C with a resistance adjustment and the 2C discharge at 60 °C.

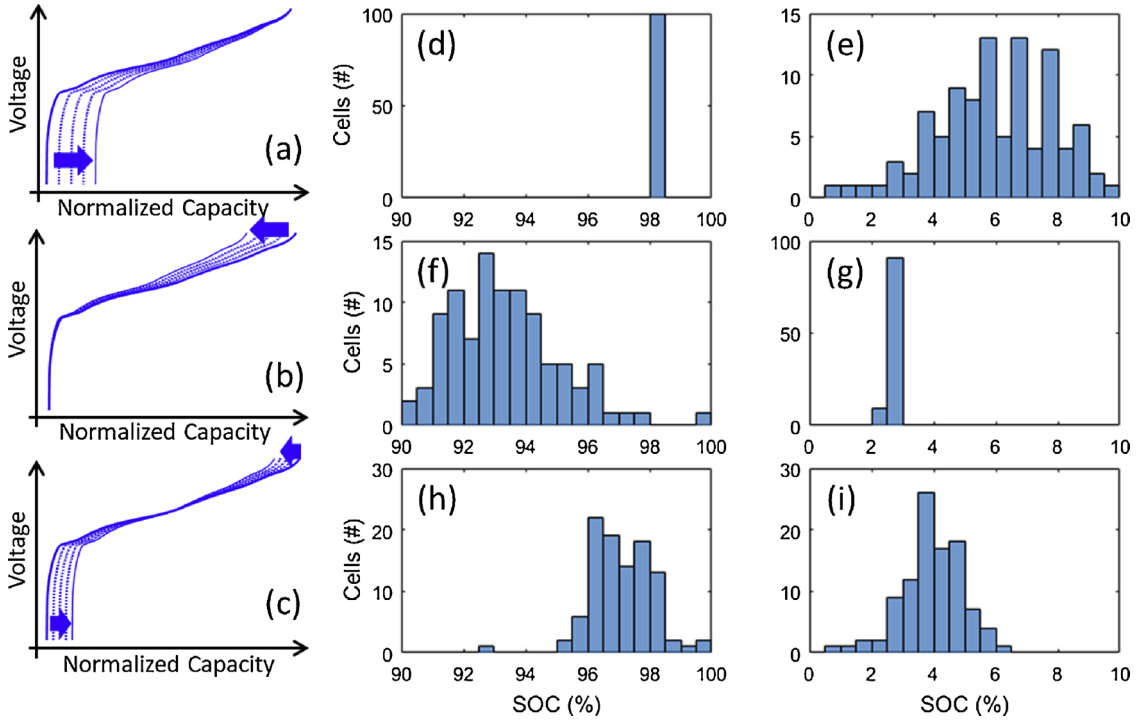

Fig. 10. Schematic representation of the impact of the degradation in discharge (a), charge (b), and 50/50 discharge/charge (c) on the OCV vs. the normalized capacity. Beginning and end of discharge SOC distribution after 25% capacity loss for a 100S1P battery pack with cells degrading up to ± 30% faster than a reference cell in a normal distribution if the degradation is occurring during discharge (d–e), during charge (f–g), and 50% in discharge and 50% in charge (h–i).

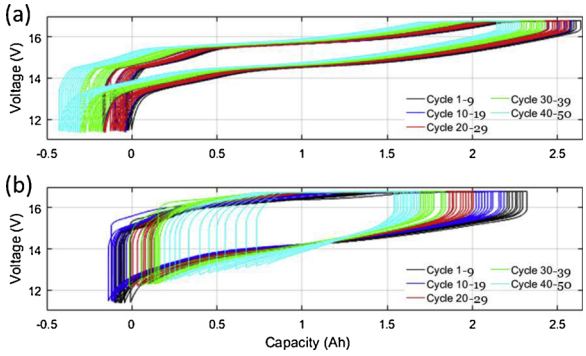

Fig. 11. Evolution of voltage vs. capacity curves without correction for 4S1P battery packs tested for 50 cycles at room temperature and 0 °C [68].

clearly visible on Fig. 12(c) where it can be seen that all the cells are similar, i.e., same IC signature, but that their initial voltage is different and lower for cells with a lower SOC. Fig. 12(b) highlights the complicated relationship at the pack level. At high voltage, the capacity usage in each SC appears shifted depending on the initial SOC, which was expected based on Fig. 12(c). The most noticeable changes are at low voltage where the last peak appears hugely broaden for some cells. This can be explained by the fact that at his stage, the cells that started at a low SOC are already fully discharged (peak is completed); whereas, the cells that started at a high SOC still have some capacity (on the peak). At the pack level, most cells finished the peak and thus have their voltage dropping sharply. As a result, there was a big dV for a small dQ. Consequently, the peak at the SC level appeared to broaden. This new graphical visualization tool for IC or DV curves, that will be referred at $IC_{SC/P}$ to differentiate it from the standard IC curve of the pack (IC_P) or of the single cells (IC_{SC}), will prove useful to quantify changes in pack voltage signature upon aging, severe imbalance, or high cell-to-cell variations more accurately. The latter will be the topic of a subsequent publication.

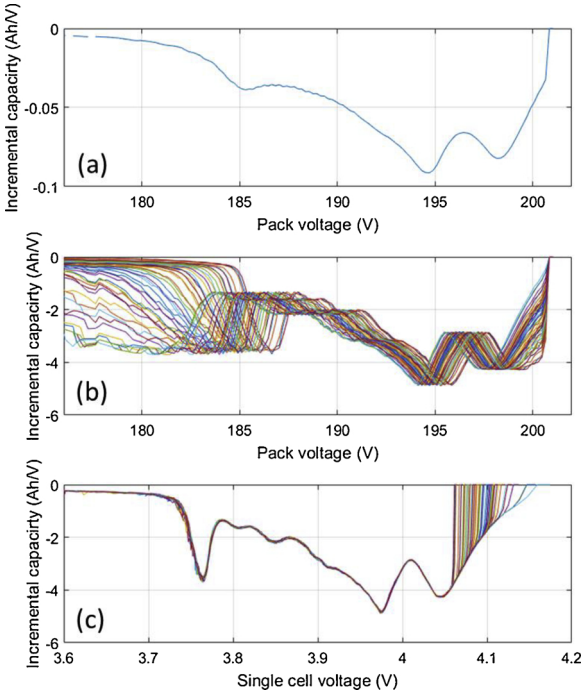

Fig. 12. (a) Incremental capacity signature of a C/25 discharge for a 49S1P battery pack with up to 10% variations on the SC initial SOC and associated incremental capacity curves for the SC vs. (b) the pack voltage, and (c) the single cell voltage. Each color corresponds to a different single cell in the 49S1P assembly.

3.5. Limitations and outlook

In its current state, this ESS model can calculate the voltage response of battery packs under many different topologies and

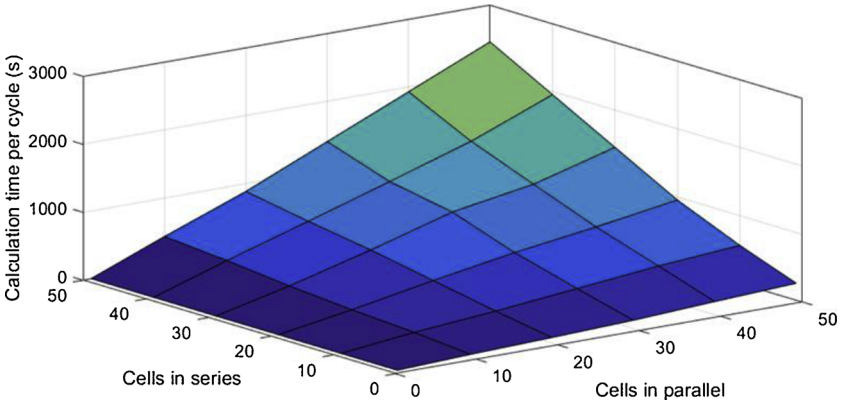

Fig. 13. Calculation time per cycle as a function of the number of cells in series and the number of cells in parallel.

degradation scenarios. However, there are still some limitations and room for improvement:

- The model does not have yet any thermal component to calculate the changes of temperature in cells (and adjacent cells) based on the applied duty cycle and the undergoing electrochemical reactions in the SCs [74–78]. However, from the modular architecture of the model, it could be integrated in the near future.

- The model can handle nSmP and mPnS topologies with modules of cells in series then paralleled or in parallel then in series. The only topology that is not supported is the one where modules consisting of cells in series and parallel are themselves in series and parallel.

- The current BMS model is quite rudimentary and does not perform some of the classic BMS calculations [79,80] such as online capacity, SOC, and SOH tracking. Work is in progress to implement the same controls that are on the BESS systems monitored by HNEI [81].

- The model is efficient for calculation in series but much slower for cells in parallel (3.5 s/cycle for 50 cells in series vs. 250 s/cycle for 50 cells in parallel at equivalent timestamps). This could become a problem for aging studies of packs with many cells in parallel. Fig. 13 presents calculation times as a function of the number of cells in series and parallel; it can be seen that for a 50S50 P pack (2500 cells), calculation time is around 2500s per cycle. Calculation times could be reduced by increasing the timestamp ε, but it was found that at least 200 points per regime result in the best accuracy and resolution for EVS [71,72]. However, the code was not optimized and could probably be hastened significantly by taking advantage of parallel computing. Other concepts to handle cells in parallel could also be investigated.

3.6. Possible applications of the model

The first application of this model will be to calculate the impact of inhomogeneities on the initial electrochemical of the assembly for different chemistries, topologies and levels of variations for the initial SOC, the maximum capacity, resistance, and the initial SOH (e.g., different levels of calendar aging prior to assembly). Future work will investigate the impact of different aging scenarios on imbalance evolution. Simulation of the degradation of HNEI deployed BESS systems based on the representative usage [81] and laboratory degradation analysis [82] will also be undertaken.

Another application could be to test the impact of a wide variety of controls and balancing algorithms [35,39,83–87] under controlled conditions and with a realistic battery model. Moreover, since the SOC and SOH are calculated for each SC independently, this approach also offers some opportunities to validate and compare further promising SOH/SOC estimation techniques such as the pala model [49] or other approaches [88–93] including Kalman filter-based ones [94] on a wide range of aging scenarios. This will remove the main drawback of most studies proposing new SOC/SOH validation methods where validation is only one set of experiments, and thus the universality of the method cannot be claimed. In addition, because of the modular approach and since every sub-model is entirely independent, alternative approaches for the SC and the pack engines could also be tested.

The investigation and the prediction of temperature inhomogeneities in battery pack based on the usage of the different SC and their impact on performance is of interest and will be investigated in the near future to provide experimental validation. Additionally, once fully parameterized, such model could find some uses other than battery research to help maintenance such as flagging underperforming module and deciphering the urgency of replacement or predicting the lifetime performance of grid or EV battery technology. Overall, it is expected to provide valuable understanding for future deployments of energy storage technologies.

4. Conclusions

In this work, a combined comprehensive approach toward battery pack modeling was introduced by combining several previously validated and published models into a coherent framework. The model is divided into three independent engines: a single cell engine, a packed engine, and a BMS engine. This modular architecture allows flexibility in the study of the impact of different parameters or different approaches for each sub-models.

The main novelty of this work is the interconnection between the sub-models allowing them to interact with one another, what adjustments were necessary compared to the stand-alone versions, and what new parameters needed to be introduced. In particular, the option to perform offline or online SOH evolution, the ability to speed up or slow down the degradation of any cells within the pack, and the possibility of choosing where the degradation occurred were implemented. This proved to be essential to be able to model the evolution of the imbalance right.

Overall, this paper introduced a new open modular framework for future modeling work on, among others, the impact of cell-to-cell variations, inhomogeneous degradation, SOC and SOH tracking, balancing and performance forecast.

Author contributions

M.D. designed and implemented the model; G.B. and C.P contributed to validation and debugging. M.D. wrote the paper with inputs and proofing from G.B., C.P., T.Y., D.W., and J.M.

Conflicts of interest

The authors declare no conflict of interest.

Glossary

BESS	Battery energy storage system
BMS	Battery management system
C	Rate
Cap	Capacitance
DV	Differential voltage
ECM	Equivalent circuit model
ESS	Energy storage system
FC	Full cell
I	Current
IC	Incremental capacity
LAM	Loss of active material
LLI	Loss of lithium inventory
LR	Loading ratio
NE	Negative electrode
OCV	Open circuit voltage
OFS	Offset
OPV	Open pack voltage
ORI	Ohmic resistance increase
PE	Positive electrode
Qr	Capacity ration
R	Resistance
RC	Rate capability
RDF	Rate degradation factor
SC	Single cell
Sf	Scaling factor
SOC	State of charge
SOH	State of health
T	Temperature
Tf	Translation factor
V	Voltage

Acknowledgments

This work was funded by the state of Hawaii, ONR Asia Pacific Research Initiative for Sustainable Energy Systems (APRISES) award number N00014-17-1-2206 and the Engineering and Physical Science Research Council (EPSRC - EP/ I01585X/1) through the Engineering Doctoral Centre in High Value, Low Environmental Impact Manufacturing in collaboration with WMG Centre High Value Manufacturing Catapult and Jaguar Land Rover.

The authors are also grateful to the Hawaiian Electric Company for their ongoing support of the operations of the Hawai'i Sustainable Energy Research Facility (HiSERF). The authors would like to thank N. Vuillaume, C. Truchot, A. Devie, and B.Y. Liaw for their contribution to the development of the sub-models used in this work.

References

[1] http://www.hawaiicleanenergyinitiative.org.
[2] http://www.honolulu.gov/cms-csd-menu/site-csd-sitearticles/985-site-csd-news-2017-cat/29848-12-12-17-hawai%CA%BBi%E2%80%99s-mayors-commit-to-shared-goal-of-100-percent-renewable-ground-transportation-by-2045.html.
[3] D. Anseán, M. Dubarry, A. Devie, B.Y. Liaw, V.M. García, J.C. Viera, M. González, Operando lithium plating quantification and early detection of a commercial LiFePO 4 cell cycled under dynamic driving schedule, J. Power Sources 356 (2017) 36–46, https://doi.org/10.1016/j.jpowsour.2017.04.072.
[4] E. Telaretti, L. Dusonchet, Stationary battery technologies in the U.S.: development Trends and prospects, Renew. Sustain. Energy Rev. 75 (2017) 380–392, https://doi.org/10.1016/j.rser.2016.11.003.
[5] E. Hittinger, J.F. Whitacre, J. Apt, What properties of grid energy storage are most valuable? J. Power Sources 206 (2012) 436–449, https://doi.org/10.1016/j.jpowsour.2011.12.003.
[6] M. Abdel-Monem, O. Hegazy, N. Omar, K. Trad, P.Vd. Bossche, J.V. Mierlo, Lithium-Ion Batteries: Comprehensive Technical Analysis of Second-Life Batteries for Smart Grid Applications vol. 2017, (2017).
[7] K. Uddin, M. Dubarry, M. Glick, The viability of vehicle-to-grid operations from a battery technology and policy perspective, Energy Policy 113 (2018) 342–347, https://doi.org/10.1016/j.enpol.2017.11.015.
[8] E. Cripps, M. Pecht, A Bayesian nonlinear random effects model for identification of defective batteries from lot samples, J. Power Sources 342 (2017) 342–350, https://doi.org/10.1016/j.jpowsour.2016.12.067.
[9] F. An, L. Chen, J. Huang, J. Zhang, P. Li, Rate dependence of cell-to-cell variations of lithium-ion cells, Sci. Rep. 6 (2016) 35051, https://doi.org/10.1038/srep35051.
[10] S.F. Schuster, M.J. Brand, P. Berg, M. Gleissenberger, A. Jossen, Lithium-ion cell-to-cell variation during battery electric vehicle operation, J. Power Sources 297 (2015) 242–251, https://doi.org/10.1016/j.jpowsour.2015.08.001.
[11] T. Baumhöfer, M. Brühl, S. Rothgang, D.U. Sauer, Production caused variation in capacity aging trend and correlation to initial cell performance, J. Power Sources 247 (2014) 332–338, https://doi.org/10.1016/j.jpowsour.2013.08.108.
[12] S. Santhanagopalan, R.E. White, Quantifying cell-to-Cell variations in Lithium ion batteries, Int. J. Electrochem. 2012 (2012) 1–10, https://doi.org/10.1155/2012/395838.
[13] J. Kim, J. Shin, Screening process of Li-ion series Battery pack for improved voltage SOC balancing, International Power Electronics Conference, (2010) 2010.
[14] K. Rumpf, M. Naumann, A. Jossen, Experimental investigation of parametric cell-to-cell variation and correlation based on 1100 commercial lithium-ion cells, J. Energy Storage (14) (2017) 224–243, https://doi.org/10.1016/j.est.2017.09.010.
[15] X. He, A facile consistency screening approach to select cells with better performance consistency for commercial 18650 Lithium ion cells, Int. J. Electrochem. Sci. (2017) 10239–10258, https://doi.org/10.20964/2017.11.01.
[16] S.J. Harris, D.J. Harris, C. Li, Failure statistics for commercial lithium ion batteries: a study of 24 pouch cells, J. Power Sources 342 (2017) 589–597, https://doi.org/10.1016/j.jpowsour.2016.12.083.
[17] M. Dubarry, N. Vuillaume, B.Y. Liaw, Origins and accommodation of cell variations in Li-ion battery pack modeling, Int. J. Energy Res. 34 (2) (2010) 216–231, https://doi.org/10.1002/er.1668.
[18] C. Zhang, Y. Jiang, J. Jiang, G. Cheng, W. Diao, W. Zhang, Study on battery pack consistency evolutions and equilibrium diagnosis for serial- connected lithium-ion batteries, Appl. Energy 207 (2017) 510–519, https://doi.org/10.1016/j.apenergy.2017.05.176.
[19] C. Pastor-Fernández, T. Bruen, W.D. Widanage, M.A. Gama-Valdez, J. Marco, A study of cell-to-Cell interactions and degradation in parallel strings: implications for the battery management system, J. Power Sources 329 (2016) 574–585, https://doi.org/10.1016/j.jpowsour.2016.07.121.
[20] Zhao, Y.; Zhang, W.; Jiang, J.; Zhao, T.; Wen, F. In Analysis on Inconsistency of Electric Bicycle Battery Pack, Transportation Electrification Asia-Pacific (ITEC Asia-Pacific), 2014 IEEE Conference and Expo, Beijing, China, 2014; IEEE: Beijing, China, 2014 1-5, 10.1109/ITEC-AP.2014.6941063.
[21] Y. Jiang, J. Jiang, C. Zhang, W. Zhang, Y. Gao, Q. Guo, Recognition of battery aging variations for LiFePO 4 batteries in 2nd use applications combining incremental capacity analysis and statistical approaches, J. Power Sources 360 (2017) 180–188, https://doi.org/10.1016/j.jpowsour.2017.06.007.
[22] V. Ramadesigan, P.W.C. Northrop, S. De, S. Santhanagopalan, R.D. Braatz, V.R. Subramanian, Modeling and simulation of lithium-ion batteries from a systems engineering perspective, J. Electrochem. Soc. 159 (3) (2012) R31, https://doi.org/10.1149/2.018203jes.
[23] Zhang, C.; Li, K.; Mcloone, S.; Yang, Z. In Battery Modelling Methods for Electric Vehicles - A Review, European Control Conference (ECC), Strasbourg, France, 2014; IEEE: Strasbourg, France, 2014; pp 2673-2678.
[24] A.U. Schmid, L. Eringer, I. Lambidis, K.P. Birke, Electrochemical balancing of lithium-ion cells by nickel-based cells, J. Power Sources 367 (2017) 49–56, https://doi.org/10.1016/j.jpowsour.2017.09.011.
[25] T.R. Ashwin, A. McGordon, P.A. Jennings, Electrochemical modelling of Li-ion battery pack with constant voltage cycling, J. Power Sources 341 (2017) 327–339, https://doi.org/10.1016/j.jpowsour.2016.11.092.
[26] M. Doyle, J. Newman, A.S. Gozdz, C.N. Schmutz, J.M. Tarascon, Comparison of modeling predictions with experimental data from plastic Lithium ion cells, J. Electrochem. Soc. 143 (6) (1996) 1890–1903.
[27] I.J. Ong, J. Newman, Double-layer capacitance in a dual Lithium ion insertion cell, J. Electrochem. Soc. 146 (12) (1999) 4360–4365.
[28] J. Christensen, J. Newman, Effect of anode film resistance on the Charge/Discharge capacity of a lithium-ion battery, J. Electrochem. Soc. 150 (11) (2003) A1416, https://doi.org/10.1149/1.1612501.
[29] Y. Merla, B. Wu, V. Yufit, R.F. Martinez-Botas, G.J. Offer, An easy-to-parameterise physics-informed battery model and its application towards lithium-ion battery cell design, diagnosis, and degradation, J. Power Sources 384 (2018) 66–79, https://doi.org/10.1016/j.jpowsour.2018.02.065.
[30] Y. Ye, Y. Shi, L.H. Saw, A.A.O. Tay, Simulation and evaluation of capacity recovery methods for spiral-wound lithium ion batteries, J. Power Sources 243 (2013) 779–789, https://doi.org/10.1016/j.jpowsour.2013.06.083.
[31] L. Tao, J. Ma, Y. Cheng, A. Noktehdan, J. Chong, C. Lu, A review of stochastic battery models and health management, Renew. Sustain. Energy Rev. 80 (2017) 716–732, https://doi.org/10.1016/j.rser.2017.05.127.
[32] G. Fan, P. K, G.L. Storti, M. Canova, J. Marcicki, X. Yang, A Reduced-Order Multi-Scale, Multi-Dimensional Model for Performance Prediction of Large-Format Li-Ion Cells, J. Electrochem. Soc. 164 (2) (2017) A252–A254, https://doi.org/10.1149/2.0791702jes].
[33] S.M. Mousavi G, M. Nikdel, Various battery models for various simulation studies and applications, Renew. Sustain. Energy Rev. 32 (2014) 477–485, https://doi.org/10.1016/j.rser.2014.01.048.
[34] M. Dubarry, N. Vuillaume, B.Y. Liaw, San Antonio TX, 2008; San Antonio TXFrom Li-Ion Single Cell Model to Battery Pack Simulation, 17th IEEE International Conference on Control Applications2008, From Li-Ion Single Cell Model to Battery Pack Simulation, 17th IEEE International Conference on Control Applications

(2008) 708–713.
[35] T. Bruen, J. Marco, M. Gama, In model based design of balancing systems for electric vehicle battery packs, IFACPapersOnLine 2015 (2015) 395–402.
[36] X. Zhang, Y. Wang, D. Yang, Z. Chen, An on-line estimation of battery pack parameters and state-of-charge using dual filters based on pack model, Energy 115 (2016) 219–229, https://doi.org/10.1016/j.energy.2016.08.109.
[37] M. Mathew, Q.H. Kong, J. McGrory, M. Fowler, Simulation of lithium ion battery replacement in a battery pack for application in electric vehicles, J. Power Sources 349 (2017) 94–104, https://doi.org/10.1016/j.jpowsour.2017.03.010.
[38] L. Zhou, Y. Zheng, M. Ouyang, L. Lu, A study on parameter variation effects on battery packs for electric vehicles, J. Power Sources 364 (2017) 242–252, https://doi.org/10.1016/j.jpowsour.2017.08.033.
[39] F. Baronti, R. Roncella, R. Saletti, Performance comparison of active balancing techniques for lithium-ion batteries, J. Power Sources 267 (2014) 603–609, https://doi.org/10.1016/j.jpowsour.2014.05.007.
[40] M. Dubarry, A. Devie, B.Y. Liaw, Cell-balancing currents in parallel strings of a battery system, J. Power Sources 321 (2016) 36–46, https://doi.org/10.1016/j.jpowsour.2016.04.125.
[41] T. Bruen, J. Marco, Modelling and experimental evaluation of parallel connected lithium ion cells for an electric vehicle battery system, J. Power Sources 310 (2016) 91–101, https://doi.org/10.1016/j.jpowsour.2016.01.001.
[42] C.-Y. Chang, P. Tulpule, G. Rizzoni, W. Zhang, X. Du, A probabilistic approach for prognosis of battery pack aging, J. Power Sources 347 (2017) 57–68, https://doi.org/10.1016/j.jpowsour.2017.01.130.
[43] J. Lee, J.-H. Ahn, B.K. Lee, A novel Li-ion Battery pack modeling considering single cell information and capacity variation, Energy Conversion Congress and Exposition (ECCE), IEEE, Cincinnati, OH, USA, 2017, pp. 5242–5247, https://doi.org/10.1109/ECCE.2017.8096880 2017; IEEE: Cincinnati, OH, USA, 2017.
[44] T. Grün, K. Stella, O. Wollersheim, Influence of circuit design on load distribution and performance of parallel-connected Lithium ion cells for photovoltaic home storage systems, J. Energy Storage 17 (2018) 367–382, https://doi.org/10.1016/j.est.2018.03.010.
[45] M. Dubarry, B.Y. Liaw, Development of a universal modeling tool for rechargeable lithium batteries, J. Power Sources 174 (2) (2007) 856–860, https://doi.org/10.1016/j.jpowsour.2007.06.157.
[46] M. Dubarry, N. Vuillaume, B.Y. Liaw, From single cell model to battery pack simulation for Li-ion batteries, J. Power Sources 186 (2) (2009) 500–507, https://doi.org/10.1016/j.jpowsour.2008.10.051.
[47] M. Dubarry, C. Truchot, B.Y. Liaw, Synthesize battery degradation modes via a diagnostic and prognostic model, J. Power Sources 219 (2012) 204–216, https://doi.org/10.1016/j.jpowsour.2012.07.016.
[48] M. Dubarry, C. Truchot, A. Devie, B.Y. Liaw, State-of-Charge determination in lithium-ion battery packs based on two-point measurements in life, J. Electrochem. Soc. 162 (6) (2015) A877–A884, https://doi.org/10.1149/2.0201506jes.
[49] M. Dubarry, M. Berecibar, A. Devie, D. Anseán, N. Omar, I. Villarreal, State of health battery estimator enabling degradation diagnosis: model and algorithm description, J. Power Sources 360 (2017) 59–69, https://doi.org/10.1016/j.jpowsour.2017.05.121.
[50] C. Truchot, M. Dubarry, B.Y. Liaw, State-of-charge estimation and uncertainty for lithium-ion battery strings, Appl. Energy 119 (0) (2014) 218–227, https://doi.org/10.1016/j.apenergy.2013.12.046.
[51] M. Dubarry, C. Truchot, M. Cugnet, B.Y. Liaw, K. Gering, S. Sazhin, D. Jamison, C. Michelbacher, Evaluation of commercial lithium-ion cells based on composite positive electrode for plug-in hybrid electric vehicle applications. Part I: initial characterizations, J. Power Sources 196 (23) (2011) 10328–10335, https://doi.org/10.1016/j.jpowsour.2011.08.077.
[52] B.Y. Liaw, G. Nagasubramanian, R.G. Jungst, D.H. Doughty, Modeling of lithium ion cells: a simple equivalent-circuit model approach, Solid State Ion. 175 (1-4) (2004) 835–839, https://doi.org/10.1016/j.ssi.2004.09.049.
[53] M.W. Verbrugge, R.S. Conell, Electrochemical and thermal characterization of battery modules commensurate with electric vehicle integration, J. Electrochem. Soc. 149 (1) (2002) A45, https://doi.org/10.1149/1.1426395.
[54] M. Dubarry, A. Devie, B.Y. Liaw, The value of battery diagnostics and prognostics, Journal of Energy and Power Sources 1 (5) (2014) 242–249.
[55] M. Kassem, C. Delacourt, Postmortem analysis of calendar-aged graphite/LiFePO4 cells, J. Power Sources 235 (2013) 159–171, https://doi.org/10.1016/j.jpowsour.2013.01.147.
[56] J.P. Schmidt, H.Y. Tran, J. Richter, E. Ivers-Tiffée, M. Wohlfahrt-Mehrens, Analysis and prediction of the open circuit potential of lithium-ion cells, J. Power Sources 239 (2013) 696–704, https://doi.org/10.1016/j.jpowsour.2012.11.101.
[57] C.R. Birkl, M.R. Roberts, E. McTurk, P.G. Bruce, D.A. Howey, Degradation diagnostics for lithium ion cells, J. Power Sources 341 (2017) 373–386, https://doi.org/10.1016/j.jpowsour.2016.12.011.
[58] J. Vetter, P. Novák, M.R. Wagner, C. Veit, K.C. Möller, J.O. Besenhard, M. Winter, M. Wohlfahrt-Mehrens, C. Vogler, A. Hammouche, Ageing mechanisms in lithium-ion batteries, J. Power Sources 147 (1-2) (2005) 269–281, https://doi.org/10.1016/j.jpowsour.2005.01.006.
[59] Schlasza, C.; Ostertag, P.; Chrenko, D.; Kriesten, R.; Bouquain, D. In Review on the aging mechanisms in Li-ion batteries for electric vehicles based on the FMEA method, Transportation Electrification Conference and Expo (ITEC), 2014 IEEE, Dearborn, MI, USA, 2014; IEEE: Dearborn, MI, USA, 2014, 10.1109/ITEC.2014.6861811.
[60] L.S. Kanevskii, V.S. Dubasova, Degradation of Lithium-Ion Batteries and how to fight it: a review, Russ. J. Electrochem. 41 (1) (2005) 1–16.
[61] A. Devie, M. Dubarry, Durability and reliability of electric vehicle batteries under electric utility grid operations. Part 1: cell-to-Cell variations and preliminary testing, Batteries 2 (3) (2016) 28, https://doi.org/10.3390/batteries2030028.
[62] S. Rohr, S. Müller, M. Baumann, M. Kerler, F. Ebert, D. Kaden, M. Lienkamp, Quantifying uncertainties in reusing lithium-ion batteries from electric vehicles, Procedia Manuf. 8 (2017) 603–610, https://doi.org/10.1016/j.promfg.2017.02.077.
[63] A. Devie, G. Baure, M. Dubarry, Intrinsic variability in the degradation of a batch of commercial 18650 lithium-ion cells, Energies 11 (5) (2018), https://doi.org/10.3390/en11051031.
[64] K. Uddin, S. Perera, W. Widanage, L. Somerville, J. Marco, Characterising lithium-ion battery degradation through the identification and tracking of electrochemical battery model parameters, Batteries 2 (2) (2016), https://doi.org/10.3390/batteries2020013.
[65] M. Dubarry, A. Devie, K. McKenzie, Durability and reliability of electric vehicle batteries under electric utility grid operations: bidirectional charging impact analysis, J. Power Sources 358 (2017) 39–49, https://doi.org/10.1016/j.jpowsour.2017.05.015.
[66] M. Dubarry, G. Baure, A. Devie, Durability and reliability of EV batteries under electric utility grid operations: path dependence of battery degradation, J. Electrochem. Soc. 165 (5) (2018) A773–A783, https://doi.org/10.1149/2.0421805jes.
[67] M. Dubarry, C. Truchot, B.Y. Liaw, Cell degradation in commercial LiFePO4 cells with high-power and high-energy designs, J. Power Sources 258 (2014) 408–419, https://doi.org/10.1016/j.jpowsour.2014.02.052.
[68] C. Love, M. Dubarry, T. Reshetenko, A. Devie, N. Spinner, K. Swider-Lyons, R. Rocheleau, Lithium-ion cell fault detection by single-point impedance diagnostic and degradation mechanism validation for series-wired batteries cycled at 0 °C, Energies 11 (4) (2018), https://doi.org/10.3390/en11040834.
[69] A.J. Smith, J.C. Burns, S. Trussler, J.R. Dahn, Precision measurements of the coulombic efficiency of lithium-ion batteries and of electrode materials for lithium-ion batteries, J. Electrochem. Soc. 157 (2) (2010) A196–A202, https://doi.org/10.1149/1.3268129.
[70] T.M. Bond, J.C. Burns, D.A. Stevens, H.M. Dahn, J.R. Dahn, Improving precision and accuracy in coulombic efficiency measurements of Li-Ion batteries, J. Electrochem. Soc. 160 (3) (2013) A521–A527, https://doi.org/10.1149/2.014304jes.
[71] I. Bloom, A.N. Jansen, D.P. Abraham, J. Knuth, S.A. Jones, V.S. Battaglia, G.L. Henriksen, Differential voltage analyses of high-power, lithium-ion cells. 1. Technique and applications, J. Power Sources 139 (1-2) (2005) 295–303, https://doi.org/10.1016/j.jpowsour.2004.07.021.
[72] M. Dubarry, V. Svoboda, R. Hwu, B.Y. Liaw, Incremental capacity analysis and close-to-equilibrium OCV measurements to quantify capacity fade in commercial rechargeable lithium batteries, Electrochem. Solid-State Lett. 9 (10) (2006) A454–A457, https://doi.org/10.1149/1.2221767.
[73] T.R. Tanim, M.G. Shirk, R.L. Bewley, E.J. Dufek, B.Y. Liaw, Fast charge implications: pack and cell analysis and comparison, J. Power Sources 381 (2018) 56–65, https://doi.org/10.1016/j.jpowsour.2018.01.091.
[74] A. Maheshwari, M.A. Dumitrescu, M. Destro, M. Santarelli, A modelling approach to understand charge discharge differences in thermal behaviour in lithium iron phosphate – graphite battery, Electrochim. Acta 243 (2017) 129–141, https://doi.org/10.1016/j.electacta.2017.05.049.
[75] A. Fortier, M. Tsao, N. Williard, Y. Xing, M. Pecht, Preliminary study on integration of Fiber optic bragg grating sensors in Li-Ion batteries and in situ strain and temperature monitoring of battery cells, Energies 10 (7) (2017) 838, https://doi.org/10.3390/en10070838.
[76] M. Farag, H. Sweity, M. Fleckenstein, S. Habibi, Combined electrochemical, heat generation, and thermal model for large prismatic lithium-ion batteries in real-time applications, J. Power Sources 360 (2017) 618–633, https://doi.org/10.1016/j.jpowsour.2017.06.031.
[77] P. Cicconi, D. Landi, M. Germani, Thermal analysis and simulation of a Li-ion battery pack for a lightweight commercial EV, Appl. Energy 192 (2017) 159–177, https://doi.org/10.1016/j.apenergy.2017.02.008.
[78] E. Hosseinzadeh, R. Genieser, D. Worwood, A. Barai, J. Marco, P. Jennings, A systematic approach for electrochemical-thermal modelling of a large format lithium-ion battery for electric vehicle application, J. Power Sources 382 (2018) 77–94, https://doi.org/10.1016/j.jpowsour.2018.02.027.
[79] K. Liu, K. Li, Q. Peng, C. Zhang, A brief review on key technologies in the battery management system of electric vehicles, Front. Mech. Eng. (2018), https://doi.org/10.1007/s11465-018-0516-8.
[80] M. Lelie, T. Braun, M. Knips, H. Nordmann, F. Ringbeck, H. Zappen, D. Sauer, Battery management system hardware concepts: an overview, Appl. Sci. 8 (4) (2018), https://doi.org/10.3390/app8040534.
[81] M. Dubarry, A. Devie, K. Stein, M. Tun, M. Matsuura, R. Rocheleau, Battery Energy Storage System battery durability and reliability under electric utility grid operations: analysis of 3 years of real usage, J. Power Sources 338 (2017) 65–73, https://doi.org/10.1016/j.jpowsour.2016.11.034.
[82] M. Dubarry, A. Devie, Battery durability and reliability under electric utility grid operations: representative usage aging and calendar aging, J. Energy Storage 18 (2018) 185–195, https://doi.org/10.1016/j.est.2018.04.004.
[83] C. Campestrini, P. Keil, S.F. Schuster, A. Jossen, Ageing of lithium-ion battery modules with dissipative balancing compared with single-cell ageing, J. Energy Storage 6 (2016) 142–152, https://doi.org/10.1016/j.est.2016.03.004.
[84] X. Pichon, J.C. Crebier, D. Riu, A. Collet, Balancing control based on States of Charge and States of Health estimates at cell level, ICCEP, Taormina, 2015, Taormina (2015) 204–211.
[85] L. Sánchez, I. Couso, J. Otero, Y. Echevarría, D. Anseán, A model-based virtual sensor for condition monitoring of Li-Ion batteries in cyber-physical vehicle

systems, J. Sens. 2017 (2017) 1–12, https://doi.org/10.1155/2017/9643279.
[86] J. Gallardo-Lozano, E. Romero-Cadaval, M.I. Milanes-Montero, M.A. Guerrero-Martinez, Battery equalization active methods, J. Power Sources 246 (2014) 934–949, https://doi.org/10.1016/j.jpowsour.2013.08.026.
[87] Probstl, A.; Park, S.; Narayanaswamy, S.; Steinhorst, S.; Chakraborty, S. In OH-Aware Active Cell Balancing Strategy For High Power Battery Packs, 2018 Design, Automation & Test in Europe Conference & Exhibition (DATE), Dresden, Germany, 2018; Dresden, Germany, 2018,.
[88] Y. Zheng, M. Ouyang, L. Lu, J. Li, Understanding aging mechanisms in lithium-ion battery packs: from cell capacity loss to pack capacity evolution, J. Power Sources 278 (2015) 287–295, https://doi.org/10.1016/j.jpowsour.2014.12.105.
[89] M. Ouyang, S. Gao, L. Lu, X. Feng, D. Ren, J. Li, Y. Zheng, P. Shen, Determination of the battery pack capacity considering the estimation error using a Capacity–Quantity diagram, Appl. Energy 177 (2016) 384–392, https://doi.org/10.1016/j.apenergy.2016.05.137.
[90] J. Li, B. Greye, M. Buchholz, M.A. Danzer, Interval method for an efficient state of charge and capacity estimation of multicell batteries, J. Energy Storage 13 (2017) 1–9, https://doi.org/10.1016/j.est.2017.05.012.
[91] M. Pathak, S. Kolluri, V.R. Subramanian, Generic model control for lithium-ion batteries, J. Electrochem. Soc. 164 (6) (2017) A973–A986, https://doi.org/10.1149/2.1521704jes.
[92] S. Peng, X. Zhu, Y. Xing, H. Shi, X. Cai, M. Pecht, An adaptive state of charge estimation approach for lithium-ion series-connected battery system, J. Power Sources 392 (2018) 48–59, https://doi.org/10.1016/j.jpowsour.2018.04.101.
[93] Z. Omariba, L. Zhang, D. Sun, Review on health management system for lithium-ion batteries of electric vehicles, Electronics 7 (5) (2018), https://doi.org/10.3390/electronics7050072.
[94] M.A. Hannan, M.S.H. Lipu, A. Hussain, A. Mohamed, A review of lithium-ion battery state of charge estimation and management system in electric vehicle applications: Challenges and recommendations, Renew. Sustain. Energy Rev. 78 (2017) 834–854, https://doi.org/10.1016/j.rser.2017.05.001.